

Model dependence of the $\pi_1(1600) \rightarrow \rho(770)\pi$ signal

Fabian Krinner for the COMPASS-collaboration

Max-Planck-Intitut für Physik, Föhringer Ring 6, 80805 München, Alemania.

Received 5 January 2022; accepted 17 February 2022

Using the large COMPASS data set on diffractive three pion production, we investigate the contradictory observations reported by previous experiments on the existence of a resonance signal in the spin-exotic wave with spin, parity and charge conjugation quantum numbers 1^{-+} . We identify a strong dependence of the result on the employed analysis model as the cause and derive a model tuned to minimize these effects. Additionally, we study the robustness of our analysis model using the approach of freed-isobar partial-wave analysis.

Keywords: Hadron spectroscopy; COMPASS experiment; partial-wave analysis; isobar model; meson resonance; exotic; $\pi_1(1600)$; $\rho(770)$.

DOI: <https://doi.org/10.31349/SuplRevMexFis.3.0308015>

1. Introduction

While mesons are most commonly modeled as $q\bar{q}$ states using the constituent quark model, other configurations of quarks and gluons are in principle allowed by QCD. Such configurations include states that consist purely of gluonic excitation (glueballs), $q\bar{q}$ state with additional gluonic excitations (hybrids), or states with higher numbers of quark-field excitations (multi-quark states).

A priori, there is no simple way to distinguish non- $q\bar{q}$ states from ordinary $q\bar{q}$ states. However, specific combinations of J^{PC} quantum numbersⁱ exist, that cannot be realized within the constituent quark model. Such combinations of quantum numbers are called *spin-exotic*. Thus, states with spin-exotic J^{PC} quantum numbers are bound to be non- $q\bar{q}$ states.

One spin-exotic candidate state that has been discussed for a long time is the $\pi_1(1600)$, which has $J^{PC} = 1^{-+}$. In particular, several analyses of its decay into $\rho(770) + \pi$ with the subsequent decay $\rho(770) \rightarrow \pi^+ + \pi^-$ have arrived at seemingly contradictory conclusions [1–5]. These analyses are based on a partial-wave analysis (PWA) of diffractively produced 3π final states, where the PWA model is constructed using the isobar model. This model describes the decay of the produced 3π intermediate state as two subsequent two-body decays with an additional intermediate 2π state appearing, called the *isobar*. The corresponding partial wave, where the $\pi_1(1600)$ resonance may appear in diffractive processes, is the $1^{-+}1^+\rho(770)\pi P$ wave, using the labeling scheme of Ref. [6]; this wave will be referred to as the “*spin-exotic wave*” throughout this article.

2. Main COMPASS result

In this work, we discuss the results of an extensive PWA of the data set on diffractive $\pi^-\pi^-\pi^+$ production collected by the COMPASS collaboration. The PWA model consists of a set of 88 partial waves and was performed independently in 100 independent bins of the invariant mass $m_{3\pi}$ of the 3π system and in 11 bins of the reduced squared four-momentum

transfer t' . An in-depth discussion of this analysis can be found in Ref. [6].

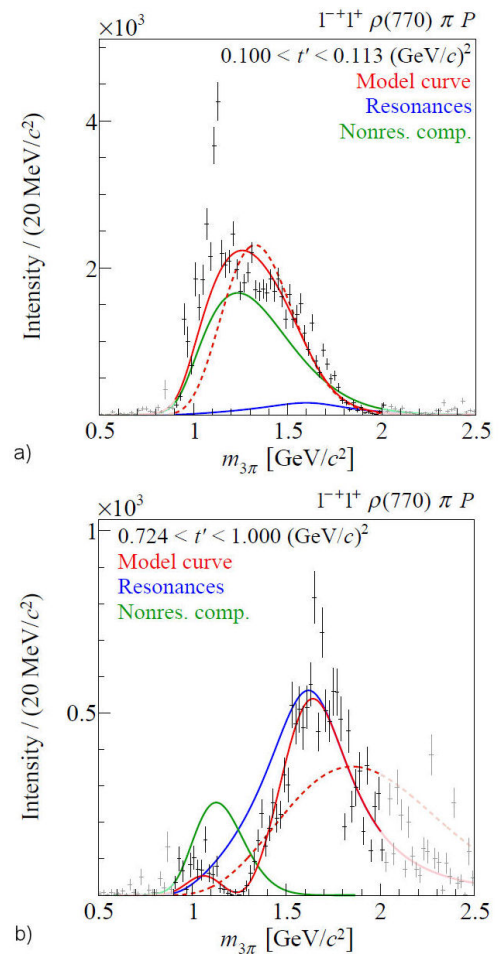


FIGURE 1. Result of the resonance-model fit of the spin-exotic wave shown for the lowest and highest t' bin. The red curve represents the full fit model, while the blue and green curves represent the interfering resonant and non-resonant components. The dashed curve shows the results of a fit, where the $\pi_1(1600)$ was omitted from the fit model.

The main result of the analysis in Ref. [7] in the spin-exotic wave is shown for the lowest and highest t' bins in Fig. 1. The measured $\pi_1(1600)$ resonance parameters are:

$$\begin{aligned} m_{\pi_1(1600)} &= 1600_{-60}^{+110} \text{ MeV}/c^2 & \text{and} \\ \Gamma_{\pi_1(1600)} &= 580_{-230}^{+100} \text{ MeV}/c^2. \end{aligned} \quad (1)$$

3. Comparison to previous results

The decay $\pi_1(1600) \rightarrow \rho(770)\pi$ has already been studied in previous analyses in particular the BNL E852 and the VES experiments as well as by COMPASS based on data using a lead target. These results are shown as blue open circles in Fig. 2 and compared to results obtained using the COMPASS

2008 data set, shown as red diamonds.

Applying the analysis models used by said previous experiments, we were able to reproduce the seemingly contradictory results for the $\pi_1(1600) \rightarrow \rho(770)\pi$ signal shown in Fig. 2. In particular, the narrow peak, attributed to a narrow $\pi_1(1600)$ in Ref. [2] turns out to be an artifact caused by missing partial waves with $J^{PC} = 2^{-+}$ in the PWA model. This effect has already been reported in Ref. [3].

We were also able to reproduce the broad structure reported in Ref. [3], where the reason for the non-observation of the $\pi_1(1600)$ resonance in this analysis is the treatment of the t' dependence. Ref. [3] only analyzes the t' range below $0.53 \text{ (GeV}/c)^2$, where we observe in Ref. [7] that the $\pi_1(1600)$ is masked by much larger, non-resonant contributions (see Fig. 1a).

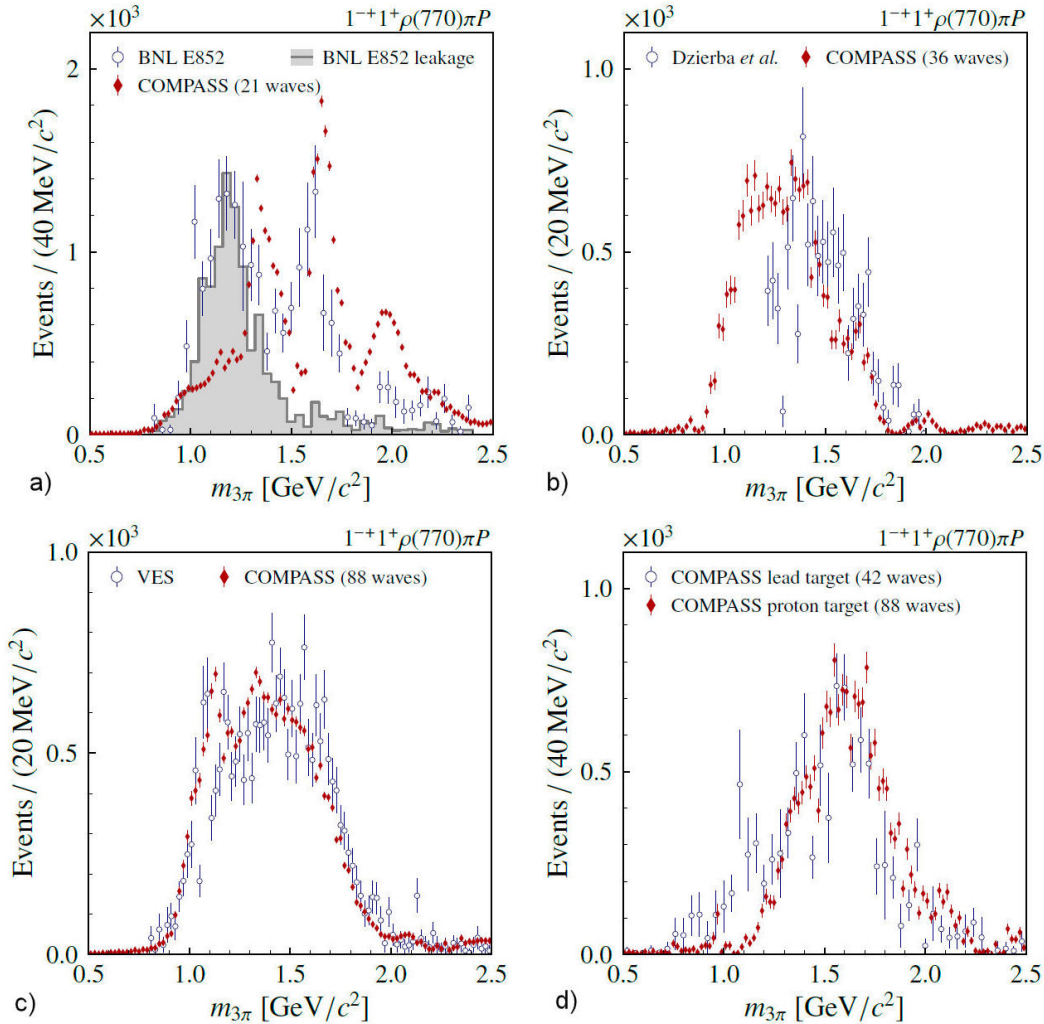


FIGURE 2. Comparison of previous results (blue open circles) taken from Fig. 18(b) of Ref. [2], Fig. 25(a) of Ref. [3], Fig. 4(a) of Ref. [4] and Fig 2(d) of Ref. [5] (left to right), to results obtained from the COMPASS data using various analysis models (red diamonds). The grey area in the left plot indicates leakage effects.

In Ref. [4] the t' region up to $1.00 \text{ (GeV}/c)^2$ was analyzed and the t' dependence was modeled using an exponential dependence in the amplitudes. This, however, still lead to the broad intensity distribution shown in Fig. 2, where no final conclusion on the existence of the $\pi_1(1600)$ could be drawn. We find a good agreement between the result of Ref. [4] and our main result of Ref. [6], summed over all 11 t' bins. Thus in Ref. [4], the $\pi_1(1600)$ resonance seems to be shadowed by non-resonant contributions, which are dominant in the low t' regions.

The comparison of the result of Ref. [5] to our main result for the highest t' bin shows a good agreement. However, we currently have no satisfying explanation, why the spin-exotic signal obtained over the full t' range taken with a lead target matches the signal in the high- t' range taken on a proton target.

In summary, we could trace back the contradictory results from previous experiments for the $\pi_1(1600) \rightarrow \rho(770)\pi$ signal to model dependences of the analysis; in particular to dependences on the set of partial waves used in the analysis and to the treatment of the t' dependence. A more detailed discussion on the differences between the mentioned analyses can be found in Sec. IV of Ref. [1].

4. Freed-isobar analysis

Even though the analysis model used in Refs. [6, 7] were constructed to minimize the model dependence of the results, several parts of the analysis still rely on model assumptions. One of the biggest remaining assumptions is the use of a fixed parameterization for the dynamic amplitudes of the $\pi^+\pi^-$ isobars, in particular the $\rho(770)$ resonance, in the PWA model. In the conventional PWA, the

dynamic amplitude of the $\rho(770)$ is modeled by a relativistic Breit-Wigner parameterization with mass and width values taken from PDG. To verify the validity of this assumption, we employ the freed-isobar approach [8], where we replace the fixed Breit-Wigner shape of the $\rho(770)$ by a set $\{\Pi_k(m_{\pi^+\pi^-})\}$ of step-like functions, with

$$\Pi_k(m_{\pi^+\pi^-}) = \begin{cases} \mathcal{F}_k, & \text{if } m_k \leq m_{\pi^+\pi^-} < m_{k+1}, \\ 0, & \text{otherwise,} \end{cases} \quad (2)$$

where the set $\{m_k\}$ are the borders of $\pi^+\pi^-$ mass ranges covering the whole kinematically allowed range for the isobar mass $m_{\pi^+\pi^-}$. This set of step-like functions approximates the value of the dynamic amplitude in every $m_{\pi^+\pi^-}$ bin by a constant value \mathcal{F}_k and each of the steps behaves like an individual partial wave in the PWA. More details on the freed-isobar approach can be found *e.g.* in Sec. V of Ref. [1]. With this approach, we are able to extract the complex-valued dynamic amplitude of the intermediate two-pion state with quantum number $J^{PC} = 1^{--}$ produced in the decay of the three-pion state with quantum numbers $J^{PC} = 1^{+-}$ directly from data in a model independent way. Since the freed-isobar approach introduces a large number of new fit parameters, we employed a coarser binning of only 50 bins in $m_{3\pi}$ and 4 bins in t' to increase statistical precision. To avoid potential leakage from other partial waves in the PWA model, whose dynamic isobar amplitudes might be described imperfectly by our fixed parameterizations, we applied the freed-isobar method not only to the spin-exotic wave, but to the twelve largest of the 88 partial waves in the PWA model simultaneously (see Table II of Ref. [1] for details). We chose the largest waves, since potential leakage from large to small waves—the spin-exotic wave being one of them—is expected to cause the largest distortions.

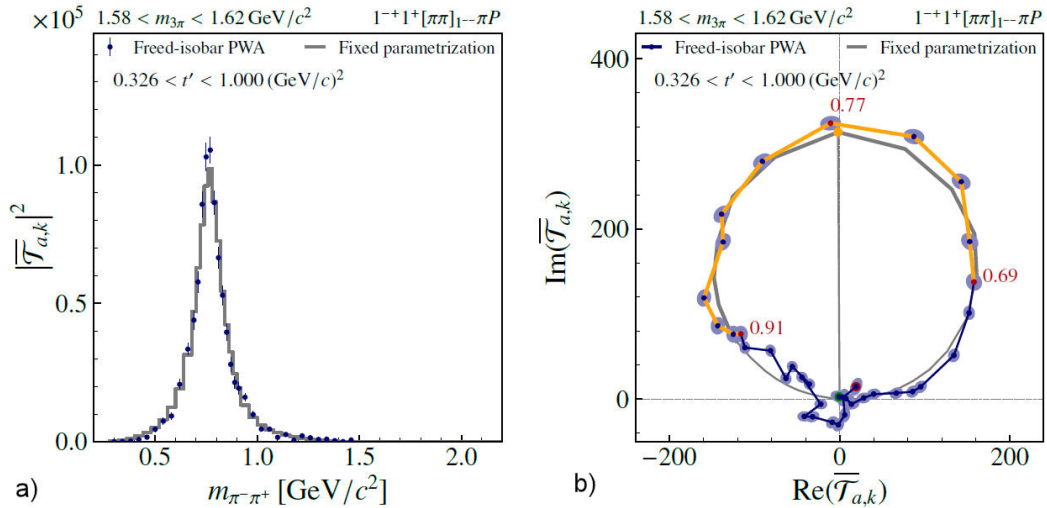


FIGURE 3. Fit result from the freed-isobar PWA in the spin-exotic wave for $1.58 < m_{3\pi} < 1.62 \text{ GeV}/c^2$ and $0.326 < t' < 1.000 \text{ (GeV}/c)^2$. The left plot shows the intensity distribution as function of the $\pi^-\pi^+$ subsystem mass. The right plot shows the same data in form of an Argand diagram. The blue points show the fit result and the grey lines represent the Breit-Wigner model for the dynamic amplitude of the $\rho(770)$ resonance in the conventional PWA.

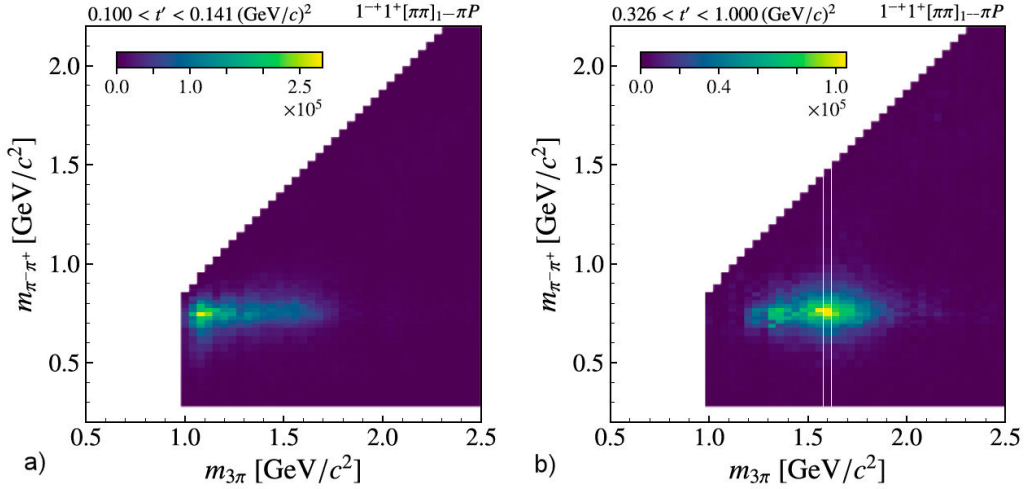


FIGURE 4. Intensity distribution of the spin-exotic wave as function of the 3π and 2π invariant mass shown for the lowest t' bin a) and the highest t' bin b). The data shown in Fig. 3 correspond to the vertical slice indicated on the right plot.

The result of this freed-isobar PWA is shown for the spin-exotic wave for a single bin in $m_{3\pi}$ and t' as blue points in Fig. 3. We see a good agreement between the extracted amplitudes and the fixed Breit-Wigner parameterization for the $\rho(770)$ used in the conventional PWA (grey lines). This shows, that the $\rho(770)$ resonance is indeed dominating the spin-exotic partial wave.

Since we performed independent freed-isobar PWA fits for all $(m_{3\pi}, t')$ cells, we can calculate the two-dimensional intensity distributions shown in Fig. 4 for the lowest and highest t' bin. While the lowest t' bin shows a broad structure in $m_{3\pi}$ corresponding to non-resonant contributions, the highest t' bin shows a clear peak at $m_{3\pi} \approx 1.6 \text{ GeV}/c^2$

and $m_{\pi^+\pi^-} \approx 0.8 \text{ GeV}/c^2$ corresponding to the decay $\pi_1(1600) \rightarrow \rho(770)\pi$. It is important to note that we have obtained this result without making any assumptions on the resonance content of neither the $J^{PC} = 1^{-+}$ three-pion state nor the $J^{PC} = 1^{--}$ two-pion state.

For a better comparison with the results from the conventional PWA obtained in Ref. [6], we coherently sum the contributions of all step-like functions comprising the dynamic isobar amplitude of the spin-exotic wave, taking into account all self-interference effects. Doing so, we obtain the intensity distribution as a function of $m_{3\pi}$ that can be compared to the result of the conventional PWA in Ref. [6]^{vi}. This compari-

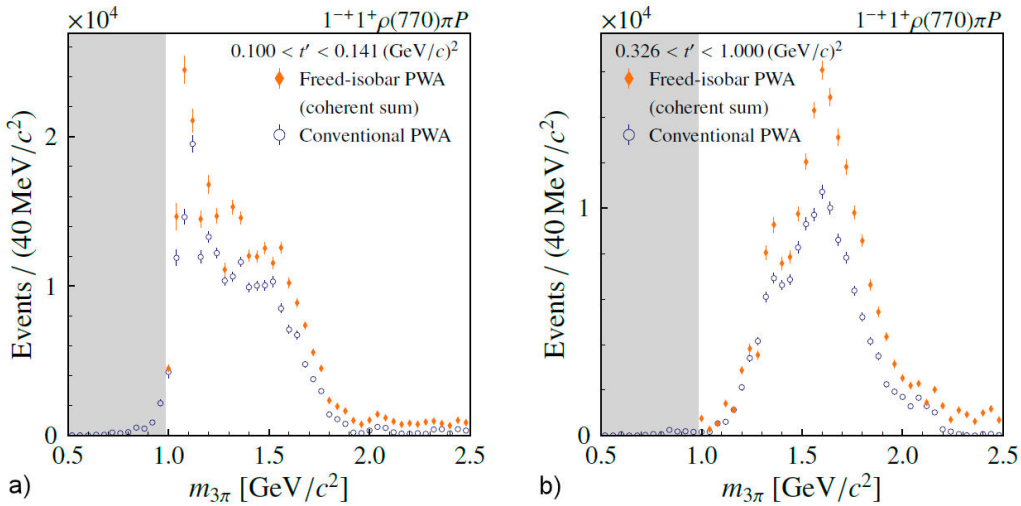


FIGURE 5. Intensity distribution of the spin-exotic wave as function of the 3π invariant mass as obtained from the freed-isobar PWA shown in orange for the lowest t' bin a) and the highest t' bin b). The intensity values are obtained by coherently summing the amplitudes in all $m_{\pi^-\pi^+}$ bins, *i.e.* along the y -axes in Fig. 4. The blue open circles represent the corresponding intensity distribution obtained from a conventional PWA with fixed parameterizations for the 2π dynamic isobar amplitude.

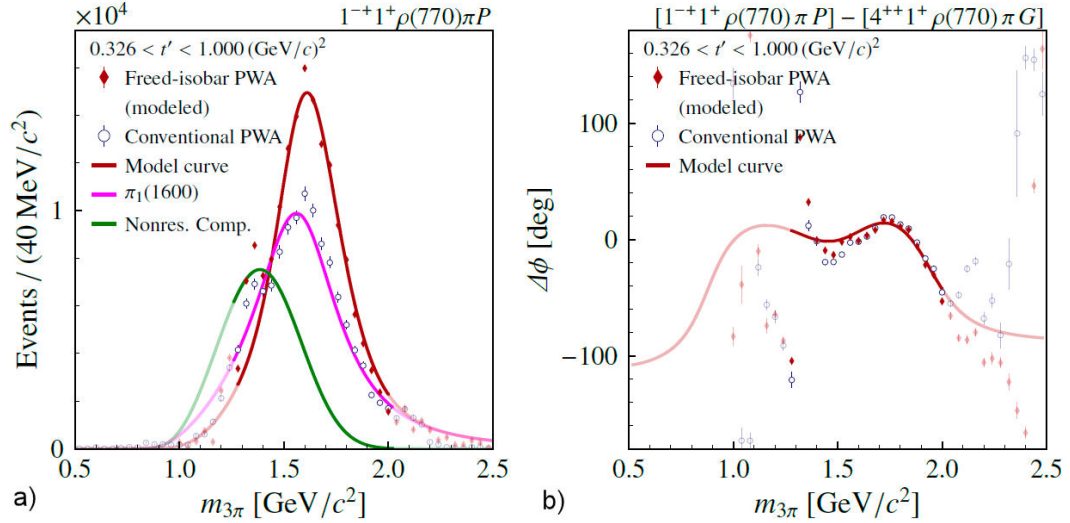


FIGURE 6. Result of the resonance-model fit amplitudes obtained from the freed-isobar PWA (red diamonds). The intensity distribution is shown on the left and the phase with respect to the $4^{++}1^+\rho(77)\pi G$ wave is shown on the right. The red curves represent the full resonance model and the magenta and green curves represent the intensity of the $\pi_1(1600)$ and the non-resonant component.

son is shown in Fig. 5 for the lowest and highest t' bin. We see that the over-all intensity distribution from the free-isobar PWA matches the result from the conventional PWA with fixed parameterizations for dynamic isobar amplitudes. However, we observe a higher total yield in the freed isobar case, which turns out not to be caused by freeing the dynamic isobar amplitude in the spin-exotic wave itself, but by freeing the dynamic isobar amplitudes in the other waves (see Table II in Ref. [1]). Nevertheless, our result confirms the validity of the assumptions made on the dynamic isobar amplitude of the spin-exotic wave in the conventional PWA in Refs. [6, 7].

As a last check of our model assumptions, we perform a fit of the $m_{3\pi}$ dependence of the transition amplitude of the three-pion system in the spin-exotic wave with the same resonance model as in Ref. [7] to obtain the resonance parameters of the $\pi_1(1600)$ from the freed-isobar PWA. This model consists of a resonant Breit-Wigner component describing the $\pi_1(1600)$ and a non-resonant component. However, for a proper resonance-model fit we need to know the phase of the 3π system with respect to a reference wave. This phase is not known from the freed-isobar PWA alone, since there a combined complex-valued coefficient is obtained for every two-pion mass range and every three-pion mass bin individually. Thus, the phases of the 3π and 2π systems are intertwined. This, in turn, requires modelling of the $\rho(770)$ resonance in order to disentangle the phases of the 3π and 2π systems. This modelling is described in detail in Sec. V C of Ref. [1] and finally allows us to perform a resonance-model fit of the spin-exotic $\pi_1(1600)$ signal from the freed-isobar PWA. The result of this fit for the highest bin in t' is shown in Fig. 6 and the resulting resonance parameters are:

$$\begin{aligned} m_{\pi_1(1600)} &= 1550 \text{ MeV}/c^2 & \text{and} \\ \Gamma_{\pi_1(1600)} &= 500 \text{ MeV}/c^2. \end{aligned} \quad (3)$$

These values are consistent with the values obtained from the conventional PWA [see Eq. (1)]. We give no uncertainties on these values, since we did not perform any systematic studies, while we expect the uncertainties to be systematically dominated. However, we estimate the uncertainties to be in the same order of magnitude as the ones given in Eq. (1).

5. Conclusion

We have presented the results of detailed studies of the $\pi_1(1600) \rightarrow \rho(770)\pi$ signal in the spin-exotic wave obtained by a comprehensive PWA using the large data set on diffractive $\pi^-\pi^-\pi^+$ production collected by the COMPASS experiment using a set of 88 partial waves. With a subsequent resonance-model fit with 14 waves, we were able to determine the $\pi_1(1600)$ resonance parameters, as given in Eq. (1).

We then compared our results for the spin-exotic wave to previously published and seemingly contradictory results. By applying previously used analysis models to our data we were able to identify the causes for the differences between the previous results. These causes are a too limited set of partial waves in the PWA model and the limited t' range that results in the $\pi_1(1600)$ resonance being masked by non-resonant contributions. These studies also led us to conclude that our analysis model is more robust with respect to such effects.

Finally, we studied the robustness of our PWA result with respect to remaining model assumptions by applying the freed-isobar approach to the spin-exotic wave, thereby removing the assumption of a Breit-Wigner fixed parameterization for the dynamic amplitude of the $\rho(770)$ isobar. Doing so, we were able to extract the dynamic isobar amplitude of the $\pi^+\pi^- P$ -wave subsystem from data and found good agreement with the assumptions made in

the conventional PWA. Thus, we were able to extract the $\pi_1(1600) \rightarrow \rho(770)\pi$ signal without any assumptions on resonance content of the 3π system and the $\pi^+\pi^-$ subsystem. We further compared the results from the freed-isobar PWA with those from the conventional PWA in Refs. [6, 7] and

find good agreement of the intensity distributions as well as the $\pi_1(1600)$ resonance parameters obtained in a resonance-model fit.

Finally, we made the full result of the freed-isobar PWA available on the HEPData platform for further analyses [9].

-
- i.* J is the spin of a state, P and C are its eigenvalues under parity and generalized charge conjugation.
 - ii.* The $m_{3\pi}$ and t' binning of the conventional PWA was adjusted to match that of the freed-isobar PWA.
1. M. G. Alexeev *et al.* [COMPASS], The exotic meson $\pi_1(1600)$ with $J^{PC} = 1^{-+}$ and its decay into $\rho(770)\pi$, <https://arxiv.org/abs/2108.01744>
 2. S. U. Chung *et al.*, [BNL E852], Exotic and q anti-q resonances in the pi+ pi- pi- system produced in pi- p collisions at 18-GeV/c, *Phys. Rev. D* **65** (2002) 072001, <https://doi.org/10.1103/PhysRevD.65.072001>.
 3. A. R. Dzierba *et al.*, A Partial wave analysis of the pi- pi- pi+ and pi- pi0 pi0 systems and the search for a $J^{PC} = 1^{-+}$ meson, *Phys. Rev. D* **73** (2006) 072001, <https://doi.org/10.1103/PhysRevD.73.072001>.
 4. A. Zaitsev *et al.* [VES], Study of exotic resonances in diffractive reactions, *Nucl. Phys.* **A675** (2000) 155, [https://doi.org/10.1016/S0375-9474\(00\)00238-4](https://doi.org/10.1016/S0375-9474(00)00238-4).
 5. M. Alekseev *et al.* [COMPASS], Observation of a $J^{PC} = 1^{-+}$ exotic resonance in diffractive dissociation of 190-GeV/c pi- into pi- pi- pi+, *Phys. Rev. Lett.* **104** (2010) 241803, <https://doi.org/10.1103/PhysRevLett.104.241803>.
 6. C. Adolph *et al.* [COMPASS], Resonance Production and $\pi\pi$ S-wave in $\pi^- + p \rightarrow \pi^- \pi^- \pi^+ + p_{recoil}$ at 190 GeV/c, *Phys. Rev. D* **95** (2017) 032004, <https://doi.org/10.1103/PhysRevD.95.032004>.
 7. M. Aghasyan *et al.* [COMPASS], Light isovector resonances in $\pi^- p \rightarrow \pi^- \pi^- \pi^+ p$ at 190 GeV/c, *Phys. Rev. D* **98** (2018) 092003, <https://doi.org/10.1103/PhysRevD.98.092003>.
 8. F. Krinner, D. Greenwald, D. Ryabchikov, B. Grube and S. Paul, Ambiguities in model-independent partial-wave analysis, *Phys. Rev. D* **97** (2018) 114008 <https://doi.org/10.1103/PhysRevD.97.114008>.
 9. See data tables in HEPData repository at <https://doi.org/10.17182/hepdata.114098>.